Functional characterization of the Co^{2+} transporter AitP in *Sinorhizobium meliloti*: a new player in Fe^{2+} homeostasis

RUNNING TITLE: AitP Fe-export orchestrates the [Fe-S] salvage pathway

Paula Mihelj[1#], Isidro Abreu[2*], Tomás Moreyra[1#], Manuel González-Guerrero[2 3], Daniel Raimunda[1]

[1]Instituto de Investigación Médica Mercedes y Martín Ferreyra - INIMEC - CONICET, UNC. Córdoba, Argentina. [2]Centro de Biotecnología y Genómica de Plantas (UPM-INIA/CSIC), Universidad Politécnica de Madrid, Madrid, Spain. [3]Departamento de Biotecnología-Biología Vegetal. Escuela Técnica Superior de Ingeniería Agronómica, Alimentaria y de Biosistemas, Universidad Politécnica de Madrid, Madrid, Spain. *Current address: Department of Biology, University of Oxford, Oxford, UK.

Abstract

Co^{2+} induces the increase of the labile-Fe pool (LIP) by Fe-S cluster damage, heme synthesis inhibition and “naked” iron import, which turns cell viability cumbersome. The N_2-fixating bacteria *Sinorhizobium meliloti* is a suitable model to determine the roles of Co^{2+}-transporting Cation diffusion facilitator exporters (Co-eCDF) in Fe^{2+} homeostasis because it presents a putative member of this sub-familiy, AitP, and two specific Fe^{2+}-export systems. An insertional mutant of AitP showed Co^{2+} sensitivity and accumulation but not Fe^{2+} sensitivity, despite AitP being a *bona fide* low affinity Fe^{2+} exporter as demonstrated by the kinetic analyses of Fe^{2+} uptake into everted membrane vesicles. Co^{2+} sensitivity was increased in double mutants lacking AitP and Fe^{2+} exporters but this did not correlate with the Co^{2+} accumulation, suggesting a concomitant Fe^{2+}-dependent induced stress. Growth in presence of sub-lethal Fe^{2+} and Co^{2+} concentrations suggested that naked Fe-import might contribute to Co^{2+} toxicity. Supporting this Co^{2+} induced transcription of Fe-import system and genes associated to Fe homeostasis. Analyses of total protoporphyrin content point to Fe-S cluster attack as the major source for LIP. AitP mediated Fe^{2+}-export is likely countered via a non-futile Fe^{2+}-import pathway. Two lines of evidence support this: i) an increased hemin uptake in presence of Co^{2+} was observed in WT *vs.* AitP mutant and ii) hemin reversed the Co^{2+} sensitivity in the last. Thus simultaneous detoxification mediated by AitP, aid cells to orchestrate an Fe-S cluster salvage response avoiding the increase in the LIP caused by disassembly of Fe-S clusters or naked iron uptake.

Importance

A cross-talk between iron and cobalt has been long recognized in biological systems. This is due to the capacity of cobalt to interfere with proper iron utilization. Cells can detoxify cobalt by exporting mechanisms involving membrane proteins known as exporters. Highlighting the cross-talk, the capacity of several cobalt exporters to also export iron is emerging. Although biologically less important than Fe^{2+}, Co^{2+} induces toxicity by promoting intracellular Fe release, which ultimately causes additional toxic effects. In this work we described how the N_2-fixating rhizobial cells solve this perturbation by clearing Fe through a Co^{2+}-exporter in order to reestablish intracellular Fe-levels by importing non-naked Fe, heme. This piggy back ride type of transport might aid bacterial cells to survive in free-living conditions were high anthropogenic Co^{2+} content could be encountered.

Introduction

Cobalt (Co) and iron (Fe) are essential micronutrients in bacteria. While Fe is broadly required to deal with biological reactions in the actual conditions ruled by dioxygen, Co is involved in a handful of metabolic pathways as catalytic cofactor or as the coenzyme vitamin B_{12} [1-3]. Due to their chemical properties, both Fe and Co become toxic under certain conditions that promote an increased bioavailability; i.e., high concentration in the extracellular environment, or in the case of Fe, increase in the exchange between intracellular storage and labile pool (*en route exchange*) [4, 5]. Although Fe accumulation seems to be curbed by Fe-storage systems recent studies have suggested that Fe accumulation might exceed their buffering capacity and lead to redox stress [6, 7].

The rhizobial α-proteobacteria and alfalfa symbiont, *Sinorhizobium melliloti*, is involved in biological N_2-fixation a process highly dependent on Fe [8]. Related to iron export in rhizobia, a P-type-IB-ATPase (Nia) has been described to be specific for Fe transport and upregulated under low O_2 conditions [9]. The membrane bound ferritin A (MbfA), a member of the CCC1 Fe efflux family, has been also described in rhizobia [10, 11]. Previous studies describing the genetic and mechanistic insights on Fe acquisition, export and storage in α-protobacteria including rhizobia [12], share in common one of the two transcriptional factors, *irr* [13] and *rirA* [14] which sense cellular Fe status through heme or Fe-S clusters, respectively. RirA regulates iron uptake genes transcription promoting naked (ferric) and non-naked (siderophore-iron complexes or heme) iron uptake in low Fe conditions. Irr regulates genes involved in heme synthesis derepressing their transcription in high Fe conditions. Cobalt is an essential nutrient for *S. meliloti* and other rhizobia [15], and an uptake system has been identified in this organism[16]. Similarly, the *dmeRF* system, consisting of a member of the FrmR family of transcriptional regulators (DmeR) and a member of the cation diffusion facilitator (DmeF),

has been involved in Co^{2+} homeostasis through export specifically during free-living stages previous to establishing symbiosis and nodulation [17-19].

A feature of Co^{2+} dyshomeostasis is related to Fe-S cluster stability. There is evidence that high Co^{2+} condition induces Fe-S cluster disassembly, triggering *suf* and *isc* machinery in response to this injure [20, 21]. Although the mechanism proposed leading to Fe-S disruption by Co^{2+} or other transition metals varies from the non-cognate metal interfering with assembly process [20], to attacking Fe-S centers in enzymes [22], the final outcome in order to supply Fe for cluster reconstitution relies on changes in the dynamic between intracellular Fe stores and labile-Fe pool (LIP) [23], and most importantly, the triggering of naked and, non-naked Fe uptake mechanisms [18, 21, 24].

In rhizobia, Fe-S cluster synthesis pathway is regulated by the transcription factor RirA, which represses the *suf* operon, the unique system for Fe-S cluster assembly in *S. meliloti*, under replete Fe conditions. RirA is a functional analog of Fur, the canonical Fe-responsive transcriptional regulator, but differs from this in that it senses Fe indirectly through an Fe-S cluster with a labile Fe as a proxy [25, 26]. Thus under low iron conditions, the release of RirA form the promoter region (IRO box) activates the transcription of the genes in its regulon. *S. meliloti* presents a second transcriptional regulator, Irr, which senses Fe status through heme binding and regulates *rirA* transcription, reinforcing *rirA* role during low iron conditions [4].

Some authors have proposed a link between Co^{2+} and Fe^{2+} homeostasis providing evidence of a RirA-mediated response upon high extracellular Co^{2+}, involving up-regulation of heme uptake systems probably as result of an increase in the inactive apo form [18]. Since Co^{2+} Fe-S clusters attack could lead to an increase in Fe^{2+} bioavailability [27-29] an Irr-mediated response is expected too.

Importantly, previously described Co^{2+} transporters are emerging as Fe-exporters in bacterial organisms [7, 30, 31]. Thus, we decided to evaluate the Fe transport capacity of SMc04167/AitP, a DmeF homolog in *S. meliloti*. Our data, showing that Co^{2+}induces

Fe dyshomeostasis by likely affecting dynamics in the LIP and that Co^{2+} sensitivity can be rescued in a non-competitively fashion by heme, together with the observations that AitP exports Fe^{2+}, allows us to propose a role for the FrmR/DmeR regulated Co^{2+} exporters of the CDF family at initial stages of the Co^{2+} induced mediated Fe-S cluster salvage pathway through Fe^{2+} export.

Results

AitP is a classical CDF Co^{2+} exporter member of a sub-family with non-unique operon architectures

A survey of more than 17.000 complete bacterial genomes allowed us to identify by Best-Reciprocal-Hit more than 759 *dmeF*/*aitP*-like genes (Fig. 1A), showing typical features of this Co^{2+} CDF subfamily. A multigene blast analysis showed that approximately 62% of these share the archetypical operon organization of juxtaposed *frmR-aitP*/*dmeR-dmeF* loci (Fig. 1A). The remaining percentage appears to have an FrmR-independent regulation with no archetypical operon configuration and no operator-promoter region for the Co^{2+} responsive transcriptional regulator FrmR/DmeR. These findings also suggest that a significant number of putative Co^{2+} exporters *aitP*-like genes might be part of Co^{2+}-responsive operons with effectors other than Co^{2+} generated when this is accumulated. Moreover, AitP-like members found in Co^{2+}-unresponsive operons could have a broaden specificitie of transport.

S. meliloti genome encodes a single member of the Co^{2+} efflux CDF subfamily (SMc04167, AitP), a homolog of the DmeF protein described in *R. leguminosarum* [17], and also of the AitP transporter of *Pseudomonas aeruginosa* [7]. As in other rhizobia, AitP is preceded by a transcriptional regulator of the FrmR/DmeR family. Phenotypic analysis of the insertional mutant of SMc04167 locus in *S. meliloti* Rm1021 (Δ*aitP* or "AitP mutant") shows increased Co^{2+} sensitivity in this strain (Fig. 1B). The sensitivity was concentration dependent and it was rescued after gene complementation (Fig. 1C). Co^{2+} accumulation occurred in the Δ*aitP* strain after incubation for 1 hour with 0.2 mM

Co^{2+} and complementation of Δ*aitP* reverted this to WT levels (Fig. 1D). Cell number after the incubation were the same in all strains indicating that this treatment (time and Co^{2+} concentrations) is sub-lethal (not shown). As expected, transcription of *aitP* and *frmR*/*dmeR* was up-regulated by Co^{2+}(Fig. 1E) but were unresponsive to Fe^{2+} (Fig. 1F) as opposed to *mbfA* (Fig. 1E-F).

AitP shows a dual specificity of transport

Bioinformatics analyses (Fig. 1A) and previous studies on AitP-like members [7] suggest an alternative role in Fe^{2+} export by AitP. As Fe^{2+} homeostasis plays a significant role for the rhizobia-legume symbiosis we decided to test whether Fe^{2+} could be transported by AitP. This could be hindered by the apparently redundant *mbfA-nia* Fe^{2+} transport systems. Thus, we heterologously overexpressed AitP in Δ*fieF E. coli* strain (not shown). FieF was previously described as an Fe^{2+} transporter [31, 32] and thus the genotypic background lacking FieF would allow measurement of Fe^{2+} with low background signal. After protein induction everted membrane vesicles were obtained and energized by pre-incubation with the electron donor NADH (or lactate) generating a H^+-electrochemical gradient (not shown). In this condition $^{59}Fe^{2+}$-importing activity to the vesicle was detected, indicating that Fe^{2+} is a substrate transported by AitP (Fig. 2A). The estimated $K_{1/2}$ value at the low milimolar range (1.35±0.21) could indicate a low affinity for transport, in line with spare strategies observed in almost all living organisms towards intracellular Fe^{2+}. The H^+-dependent transport at saturating concentrations (Fe^{2+} = 2mM) was inhibited only by Co^{2+} indicating that a competition at the transport site is possible (Fig. 2B). However, Co^{2+} accumulation observed in AitP mutant (Fig. 1D), suggests a dual (Fe/Co) transport specificity, with both ions as cytosolic substrates, exported likely by a sequential mechanism involving binding to the same transport site. Considering the absence of Fe^{2+} regulation in *aitP* transcription, these results suggests a role for AitP in Fe^{2+} transport in conditions where a concomitant intracellular Co^{2+} accumulation occurs.

AitP participates in Fe-homeostasis

Previous phenotypical characterizations of *aitP*-like genes in other rhizobial organisms point to a similar role of AitP in Co^{2+} export and detoxification [17-19] and we have previously shown that AitP homolog in *P. aeruginosa* is involved in Fe^{2+} homeostasis [7]. However, a P-IB-type ATPase, *nia*, has been described to participate in Fe^{2+} homeostasis in this organism [9] and the identification of an *mbfA* ortholog in Rm1021 genome, led us to hypothesize that AitP in *S. meliloti* would play a non-classical role in Fe^{2+} homeostasis. In this line Fe^{2+} sensitivity was not observed in Δ*aitP* strain pointing to *nia* and *mbfA* as major exit routes for Fe^{2+} in rhizobia. As Co^{2+} transport through Fe^{2+} exporters has been described we conducted phenotypical analyses in order to test whether double mutants showed increased sensitivity towards Co^{2+}. We observed an increased sensitivity in double mutants Δ*aitP*-Δ*nia* and Δ*aitP*-Δ*mbfA* beyond the threshold shown by Δ*aitP* strain (Fig 3A) but interestingly no significant increases of Co^{2+} accumulation *vs*. the Δ*aitP* strain were observed (Fig. 3B). Supporting the exclusive participation of AitP in Co^{2+} efflux, Co^{2+}-dependent *nia* transcription is not expected [9] and *mbfA* was not induced by Co^{2+} (Fig. 1E). Thus we hypothesized a possible Fe^{2+}-induced toxic effect being added to those promoted by Co^{2+} accumulation. To test this, we measured the Co^{2+} sensitivity of the Δ*aitP* *vs*. Rm1021 in presence of Fe. The increased sensitivity shown by Δ*aitP* in this condition (Fig. 3C) indicates that Co^{2+} accumulation induces a shift in iron distribution with increased LIP or higher levels of Fe^{2+} bioavailability that result toxic to the cell. As the LIP can be fed with intracellular and extracellular Fe sources we compared the transcription of *fbpA,* the substrate binding protein of the ferric cation ABC transporter, in WT and AitP mutant exposed to sub-lethal Co^{2+} concentrations, as a proxy of extracellular Fe contribution. We detected a significant increase of *fbpA* in both strains (Fig. 3D) with higher levels in AitP mutant, indicating that Fe import and likely intracellular Fe contribute to Co^{2+} toxicity. Considering that the Co^{2+} sensitivity of double mutants was observed in media with no Fe addition (ca. 10 µM total Fe) we tested the effect of Co^{2+} on pathways which inhibition could lead to an increase in the bioavailability of iron. As Co^{2+} inhibits heme synthesis and induces Fe-S

disassembly, thus promoting the increase of LIP, we quantified total protoporphyrin content in both strains exposed or not to sub-lethal Co^{2+} (Fig. 3E) and meassure the transcription of *sufA* in WT, a gene upregulated in response to Fe-S cluster attack. Although Co^{2+} treatment decreases the level of protoporphyrin, this is similar in both strains suggesting that the Co^{2+} mediated Fe-S cluster attack is the main contributing source to LIP. Regarding this, we observed *sufA* up-regulation in WT in presence of sub-lethal Co^{2+} concentrations (Fig. 3F). We analyzed also the Co^{2+}-dependency of transcriptional levels of bacterioferrtin (*bfr*) and bacterioferrodoxin (*bfd*) [33], as an estimate of the Fe storage status and the RirA mediated response. Only *bfd* transcription was increased by Co^{2+} (Fig. 3F). Finally, Fe-S cluster or heme synthesis disruption would lead to an increased Fe^{2+} bioavailability and a suitable proxy to test this are the *mbfA* and *bfr* transcriptional levels, but increases were non statistically significant (Fig. 1E and 3F).

AitP Fe^{2+} transport orchestrates the initial stages of Co^{2+} induced Fe-S cluster salvage pathway

As Co^{2+}-dependent Fe^{2+} toxic effects seem mainly related to Fe-S clusters the AitP function might be related to driving a concerted RirA dependent Fe-S cluster salvage/synthesis pathway. If Co^{2+} accumulation led to Fe-S disassembly we hypothesized that genes regulated by RirA might be dis-regulated, similar to that observed for *fbpA* and *sufA* (Fig 3D and F). In particular, SMc02726 or *shmR*, a hemin binding outer membrane receptor [34] is induced in low Fe conditions and in a Δ*rirA* mutant [35]. We detected increased transcripts of the outer membrane porin ShmR and the periplasmic component, HmuT, of the ABC-heme importer HmuTUV [36](Fig. 4A). This upregulation of heme uptake system in Δ*aitP* mutant suggested an exacerbated response to Co^{2+} accumulation likely due to an induced shift in the equilibrium of RirA towards the apo-form. We then tested if hemin addition into the media affected the Co^{2+} sensitive phenotype detected in the Δ*aitP* strain. As shown in Fig. 4B, hemin addition to

buffered TY medium (pH = 6,5) with 0.2 mM Co^{2+} rescued the Co^{2+}-sensitive phenotype at concentrations between 50-200 µM. Chelation of Co^{2+} by Fe-protoporphyrin IX (hemin) or metal exchange was discarded as empty protoporphyrin IX (PPIX) at 200 µM did not decreased Co^{2+} sensitivity (Fig. 4C). The detection of increased transcripts of hemin transport systems in Co^{2+} treated cells led us to test the hemin uptake rate under the same treatment. Surprisingly, the AitP mutant did accumulate hemin at a significant lower rate *vs.* WT (Fig. 4D and E). Although counterintuitive, this result indicates that an Fe/Co-dependent post-transcriptional regulation is possible. Overall, the data point to a role for AitP in Fe export under Co rich conditions in order to concert a RirA-dependent heme uptake process likely used for Fe-S cluster assembly.

Discussion

Cobalt is an essential element for life, and organisms like *S. meliloti* has a special requirement for Co for the methionine synthesis [15, 16]. But yet, when in high concentration it results toxic to cells. Co^{2+} efflux transporters of the CDF family have been previously characterized in rhizobia, and their transcriptional regulation is mainly governed by a FrmR/DmeR transcription factor [17]. Our bioinformatics analyses show that a significant number of members of this family might be regulated by different factors, thus responding to other effectors. Interestingly several of these members appear under the regulation of the Multiple Antibiotic Resistance Regulator (MarR) superfamily of transcription factors. Although the analysis of the functional roles of non-FrmR regulated Co^{2+}-CDF is beyond the scope of this work, the heterogeneity in *aitP*-like homologs regulation points to their capacity to transport other divalent cations. Recent works have expanded the substrate of the Co^{2+} efflux CDF transporters [7], and in this work, we have confirmed unequivocally the Fe^{2+} transporting capacity of AitP by $^{59}Fe^{2+}$ transport assays in energized everted vesicles. Due to the sensitivity of the mutant to high Co^{2+} but not Fe^{2+}, from a physiological perspective three questions arises: why AitP exports iron? And why is regulated by Co^{2+}?

The main toxic effect of Co^{2+} in bacteria seems related to Fe-S clusters assembly [20]. In *E. coli* the responses to the intoxication involves the induction of Fe-S cluster salvage pathway in order to counterbalance this effect, but also, a down regulation of naked-Fe import systems, such as Feo [23]. On the contrary, *S. meliloti*, and likely all α-proteobacteria of the *Rhizobiaceae* clade bearing RirA homologs, handle Co^{2+} toxicity by inducing iron uptake mechanisms, i.e., triggering an Fe-starvation like response. In *Agrobacterium tumefaciens*, RirA represses genes related to naked and non-naked Fe uptake and the repression is lost in presence of Co^{2+} [18]. Our results also point to an induction of expression of these iron uptake systems by Co^{2+} (*fbpA*, *shmR* and *hmuT*; Fig 3D and 4A). Similarly, this is prompted by a derepression involving Co^{2+} attack to holo-RirA.

It has been proposed that Fe-S cluster attack might lead to increase of labile-Fe pool (LIP). In the presence of Co^{2+} intoxication and accumulation, the contribution of Fe from Fe-S cluster to the LIP could be detrimental by oxidative damage. We detected *suf* up-regulation induced by Co^{2+} which is in line with increase. This could be an important Fe source in low iron conditions likely contributing to the increase sensitivity observed in double mutants lacking the main Co^{2+} efflux system and one of the Fe^{2+} exporting system (Fig 3A). As AitP-like members are also found in δ-proteobacteria which mostly regulates Fe homeostasis via direct sensing by Fur, Fe^{2+} export activity might be required to promote apo-Fur and the Fe-starvation response through non-naked Fe import.

Thus AitP activity counterbalance the increase of LIP coming both from the release of Fe from Fe-S clusters disassembled by Co^{2+} and from the Fbp-mediated e entry. The last, although represents an apparent futile Fe import-export cycle, it is only promoted by Co^{2+} accumulation. In agreement with our hypothesis, addition of naked iron increased Co^{2+} toxicity in the AitP mutant (Fig. 3C), whereas the non-naked iron from hemin had a protective role (Fig. 4B,C) likely allowing the replenishment of the intracellular pool but without incurring in a stress for the bacteria.

Two more plausible, but still speculative mechanisms, involves RirA and the regulatory protein *hmuP*/*hemp* [37]. Direct attack of RirA by Co^{2+} explains the transcriptional derepression observed of Fe-S cluster salvage (Fig. 3F) and hemin uptake genes (Fig 4A), but still leaves Fe export role for AitP dispensable. A role in the fine tuning of the Co^{2+} toxic response involving Fe-export by AitP might be explained considering the post-transcriptional regulation of *shmR* in rhizobia [38]. A unique putative binding site for the HmuP protein (a regulatory protein of *shmR*), was found in 5´UTR of *shmR* transcripts. Importantly, heme binding to HmuP has been shown *in vitro* [39]. We speculate that *in vivo* HmuP sensing capacity, likely via naked-Fe or PPIX binding, might be involved in the post-transcriptional regulation of *shmR*. Thus a LIP increase in the AitP mutant downregulates *shmR* expression. Our data showing lower hemin uptake capacity of AitP mutant *vs*. WT, even when transcripts are elevated support this. The recovery of Co^{2+} resistance in presence of high hemin concentrations (Fig. 4B) points to an unspecific uptake, or passive diffusion, mechanism in the AitP mutant. These hypotheses are currently being tested.

Based on the above, we propose a model during Co^{2+} dyshomeostasis in which AitP would detoxify both Co^{2+} and Fe^{2+}. This dual export allows cells to reduce the primary stressor (Co^{2+}) while maintaining the labile-Fe pool in range despite the release of free Fe from the Fe-S clusters or the entry of naked Fe via ABC transporter. The lack of heme import activity even when transcripts of the importing systems are high suggests that AitP activity is involved in the orchestration of the transcription-translation process of ShmR and Hmu. Future studies will focus on the role of AitP-like members on the regulation of heme uptake systems and the requirement of other partners to achieve this regulation.

Materials and methods

Bioinformatic analyses

In order to analyze the relative abundance of canonical "FrmR-AitP" operon architecture, *S. meliloti* AitP (SMc04167/ SM_RS10235) homologs were searched by the best reciprocal hit method (REF). Briefly, a database was created locally with all protein sequences from bacteria with complete genome (17,972) and chromosome (2,570) assembly level obtained from ftp://ftp.ncbi.nih.gov/genomes/refseq/bacteria/assembly_summary.txt (August 2021). A BLAST search in this database with WP_010969625.1 (SMc04167/ SM_RS10235) as query and an Expect-value of 1.10^{-5} resulted in 13,570 subject/hits. Removal of duplicated subject/hits by accession number led to 4,431 SMc04167 homolog candidates. These were blasted against *S. meliloti* 1021 (GCF_002197445.1_ASM219744v1_protein.faa) individually. In all cases BLAST retrieved WP_010969625.1 as subject, confirming best-reciprocal-hits association. After visual inspection of the subject annotations CDFs lacking the canonical poly-histidine stretch sequence (TMS4 and TMS5) were excluded in order to minimize the number of arbitrarily defined "true candidates" (Expect-value<$2.19.10^{-35}$ and percentage of positive-scoring matches>54%). Assemblies of bacterial genomes having AitP-like members with unique accession numbers were 1,651. This number of organisms reflects several strain assemblies of the same organism and we maintained it in order to promote the sensitivity of the final assessment. These were used later to compare and create a list of 759 non-redundant bacterial organisms having, or not, the FrmR-AitP architecture. The FrmR-AitP architecture search was performed using Multigenblast [40]. For the analyses here the genomic database was built with approximately 4,200 genebank formatted (.gbbf) assemblies of chromosome and complete genome with equal gender and specie names as those drew from the 1,651 organisms within the AitP list. SMc04168-SMc04167 sequence was used to run the analyses. Results were parsed to obtain the final list of

organism names with the operon architecture (~500) and compared to the list of the AitP-having organisms (~800). The remaining organisms with non-FrmR-AitP-like architecture (~300) were further analyzed. Three search strategies were followed in order to confirm the lack of FrmR(RcnR/DmeR) dependent-regulation in those organisms with AitP-like members lacking the FrmR-AitP architecture. In the first, the 500bp up-stream CDS region were downloaded and used in a tblastn search using as query the protein sequence of SMc04168/*dmeR*. In the second, protein accession numbers of AitP-like members of this group were used to retrieve the up- and downstream loci annotations using the E-fetch “identical protein group” tool. A third strategy consisted in performing a blastn search in the 500bp upstream regions for the consensus FrmR consensus binding motif using as query the *dmeR* binding sequence up-stream SMc04167 (AAATAGGGTACCCCCCTATGCT). These searches allowed us to identify 27 non-FrmR-AitP-like previous candidates as false negatives, and to confirm that 284 AitP-like loci lack the FrmR-AitP architecture. After removal of duplicated organism names, a Venn-diagram was prepared with these numbers.

Culture media, strains and mutant constructions

S. meliloti strains (Table 1) were cultured in TY media (0.5% tryptone, 0.3% yeast extract, 0.09% $CaCl_2$) supplemented with streptomycin 600 µg/ml. *S. meliloti* strain Rm1021(StrR) and *E. coli* S17-1 [41] carrying the plasmid pK19mob2ΩHMB for the mutation of SMc04167 were obtained from University of Freiburg, Germany (Table 1). The deletion mutant strain of gene SMc04167 (Δ*aitP*) was generated by plasmid insertion following described protocols [42]. Briefly, freshly grown *S. meliloti* Rm1021 were mixed with *E. coli* S-17 cells bearing the plasmid pK19mobΩHMB containing the internal sequence of the gene SMc04167, named S17-1.PI.G1PELR20F8 (www.rhizogate.de (GenDB)), and then incubated overnight at 30 °C on a nitrocellulose filter disk placed on top LB-agar. Conjugants were recovered from the filter and selected by plating on TY-agar supplemented with kanamycin 50–200 µg/ml. Complementation

was achieved by conjugation of Δ*aitP* with the non-integrative plasmid pJB3Tc20-P_{770}-*aitP* containing gene SMc04167 plus 770 bp upstream. Conjugants were selected on TY media with kanamycin (200 µg/ml) and tetracycline (10 µg/ml). Single and double mutants of *nia* (SMa1163) and *mbfA* (SMc00359) were generated by conjugation and single crossover of plasmid pJQ200SK containing a 600 bp internal region of each loci in Rm1021 (single mutant) or Δ*aitP* (double mutants). Conjugants were selected in TY agar supplemented with gentamycin (50 µg/ml). All strains were checked by PCR using purified genomic DNA as a template.

Sensitivity tests

Serial dilutions (10 µl) of *S. meliloti* Rm1021, Δ*aitP*, Δ*mbfA*, Δ*nia,* Δ*aitP*-Δ*mbfA* and Δ*aitP*-Δ*nia* cells initially at OD_{600nm}=0.4 were spotted on TY-agar supplemented with the indicated transition metals (as chloride salts, except Fe^{2+} as sulphate) concentrations for 48 h at 30°C. When hemin or PPIX (dissolved in 50 mM NaOH) were added to the media the pH was buffered with MES-KOH 15 mM pH 6.5, and the control conditions (0 mM hemin, 0 mM PPIX) were supplemented with the same amounts of NaOH.

Cobalt accumulation assays

Cells were incubated with 0.1 mM $CoCl_2$ for 1 hour for 30 minutes in TY medium during early exponential phase growth. Cells were pelleted and washed with 0.9% NaCl and mineralized with HNO_3. Co was quantified by ICP-MS or Atomic absorption spectroscopy.

Transcriptional analyses by qRT-PCR

Fold change expression levels ($2^{-\Delta\Delta Ct}$) of iron exporters and iron-related genes were assayed under 20 µM, 100 µM or 200 µM $CoCl_2$ and low (0.75 mM 2,2'-bipyridyl (Bpy), or high (0.75 mM $FeSO_4$) Fe^{2+} conditions *in vitro vs.* 16S reference gene. Cells were grown till mid-log phase at 30ºC in TY. After this the culture volume was split, supplemented or not, and incubated for 45 min at 30ºC before RNA extraction. Primers used are described in Table 1.

Iron transport assay

Fe^{2+} uptake was measured in energized everted membrane vesicles obtained from *E. coli* Δ*fieF* expressing AitP. Δ*fieF* was constructed as previously indicated [43]. Previous to transport measurement 10 µl vesicles (or the equivalent to 100 µg total protein of EMV) were energized in 100 µl of transport buffer (100 mM HEPES-Na, 250 mM sucrose, 50 mM KCl, 2 mM $MgCl_2$, 5 mM TCEP, pH 6.8) by 2-minute pre-incubation with 2.5 mM NADH in at 37 ºC and the uptake was initiated by addition of a 10-fold concentrated $^{59}Fe^{2+}$ solution and mixing. Reaction was stopped after 5-minute incubation at the same temperature by filtering through 0.22 µm nitrocellulose. Filters were immediately washed with a standard solution containing 2 mM EDTA and dissolved in scintillation cocktail for counting.

Hemin uptake assay

Hemin uptake was estimated following a previously described protocol [44]. Briefly, stationary phase cells cultured in 50 ml of TY medium were incubated for 2 hours with 0.2mM $CoCl_2$. Cells were centrifuged, washed once with ice-cold phosphate-buffered saline (PBS) pH 7.45 and resuspended in 50 ml PBS 0.05 mM $CoCl_2$ supplemented with 30 ug/ml of a hemin solution. At 2.5, 5, 15, 30, 60 and 120 minutes one milliliter of culture was centrifuge and the supernatant collected to measure the absorbance at 400 nm. No significant difference was observed in cell number of WT and AitP mutant strains after treatment, indicating that the incubation time with Co^{2+} used does not affect cell viability.

Porphyrin quantification

Porphyrins quantified following described protocol [45]. Briefly, mid-log phase cells cultured in 50 ml of TY medium were incubated for 2 hours with or without 0.2mM $CoCl_2$. Cells were centrifuged, washed twice with ice-cold 50 mM Tris-HCl (pH 8.0), resuspended in ethyl acetate/glacial acetic acid (3:1, v/v) to 1/100 the original culture volume, and lysed by sonication on ice. Cell debris was removed by centrifugation at room temperature, and the non-aqueous (top) phase was washed twice with 1 ml ddH_2O

to remove residual water-soluble contaminants. Extraction of porphyrins from the solution was achieved by the addition of 0.5 ml 3 M HCl, and the absorbance of the bottom-aqueous phase was assessed at 408 nm. Porphyrin levels were normalized to optical cell density (OD_{600nm}). No significant difference was observed in cell number of WT and AitP mutant strains after treatment, indicating that the incubation time with Co^{2+} used does not affect cell viability.

Conflict of interest statement

All authors declare that research was conducted in the absence of any commercial or financial relationships.

Author contributions

Conceived and designed the experiments: D.R., M.G.-G, I.A., P.M., T. M.

Analyzed the data: D.R., M.G.-G, I.A., P.M., T. M.

Contributed reagents/samples/analysis/tools: D.R., M.G.-G, I.A., P.M., T. M.

Wrote or edited the manuscript: D.R., M.G.-G, I.A., P.M., T. M.

All authors read and approved the final manuscript.

Funding

This work was supported by the Agencia Nacional de Promoción Científica y Tecnológica (ANPCyT)(PICT2015-2897 and PICT2018-03139 to D.R.). D.R. is a Consejo Nacional de Investigaciones Científicas y Tecnológicas (CONICET) investigator. P.M. is recipient of a CONICET doctoral fellowship. T.M. is recipient of a doctoral fellowship from ANPCyT (PICT2018-03139). I.A. was recipient of a Juan de la Cierva-Formación postodoctoral fellowship from Ministerio de Ciencia, Innovación y Universidades (FJCI-2017-33222).

Abbreviations

TM, transition metal; CDF, cation diffusion facilitator; TMS, transmembrane segment; LIP, labile-Fe pool; ICP-MS, inductively coupled plasma mass spectrometry.

Acknowledgments

We thank Dr. J.M Argüello for help and support on the setting of $^{59}Fe^{2+}$ transport assays.

References

1. Fraústo da Silva, J.J.R. and R.J.P. Williams, *The biological chemistry of the elements : the inorganic chemistry of life*. 2nd ed. 2001, Oxford: Oxford University Press. xvii, 575 p.
2. Kobayashi, M. and S. Shimizu, *Cobalt proteins.* Eur J Biochem, 1999. **261**(1): p. 1-9.
3. Okamoto, S. and L.D. Eltis, *The biological occurrence and trafficking of cobalt.* Metallomics, 2011. **3**(10): p. 963-70.
4. Bradley, J.M., et al., *Bacterial iron detoxification at the molecular level.* J Biol Chem, 2020. **295**(51): p. 17602-17623.
5. Pi, H. and J.D. Helmann, *Ferrous iron efflux systems in bacteria.* Metallomics, 2017. **9**(7): p. 840-851.
6. Guan, G., et al., *PfeT, a P1B4 -type ATPase, effluxes ferrous iron and protects Bacillus subtilis against iron intoxication.* Mol Microbiol, 2015. **98**(4): p. 787-803.
7. Salusso, A. and D. Raimunda, *Defining the Roles of the Cation Diffusion Facilitators in Fe(2+)/Zn(2+) Homeostasis and Establishment of Their Participation in Virulence in Pseudomonas aeruginosa.* Front Cell Infect Microbiol, 2017. **7**: p. 84.
8. Abreu, I., P. Mihelj, and D. Raimunda, *Transition metal transporters in rhizobia: tuning the inorganic micronutrient requirements to different living styles.* Metallomics, 2019. **11**(4): p. 735-755.
9. Zielazinski, E.L., et al., *Sinorhizobium meliloti Nia is a P(1B-5)-ATPase expressed in the nodule during plant symbiosis and is involved in Ni and Fe transport.* Metallomics, 2013. **5**(12): p. 1614-1623.
10. Bhubhanil, S., et al., *Roles of Agrobacterium tumefaciens membrane-bound ferritin (MbfA) in iron transport and resistance to iron under acidic conditions.* Microbiology (Reading), 2014. **160**(Pt 5): p. 863-871.
11. Sankari, S. and M.R. O'Brian, *Synthetic Lethality of the bfr and mbfA Genes Reveals a Functional Relationship between Iron Storage and Iron Export in Managing Stress Responses in Bradyrhizobium japonicum.* PLoS One, 2016. **11**(6): p. e0157250.
12. Rodionov, D.A., et al., *Computational reconstruction of iron- and manganese-responsive transcriptional networks in alpha-proteobacteria.* PLoS Comput Biol, 2006. **2**(12): p. e163.
13. Hamza, I., et al., *The bacterial irr protein is required for coordination of heme biosynthesis with iron availability.* J Biol Chem, 1998. **273**(34): p. 21669-74.
14. Todd, J.D., et al., *RirA, an iron-responsive regulator in the symbiotic bacterium Rhizobium leguminosarum.* Microbiology (Reading), 2002. **148**(Pt 12): p. 4059-4071.
15. Watson, R.J., et al., *Sinorhizobium meliloti cells require biotin and either cobalt or methionine for growth.* Appl Environ Microbiol, 2001. **67**(8): p. 3767-70.
16. Cheng, J., et al., *An ABC-type cobalt transport system is essential for growth of Sinorhizobium meliloti at trace metal concentrations.* J Bacteriol, 2011. **193**(17): p. 4405-16.
17. Rubio-Sanz, L., et al., *Functional and expression analysis of the metal-inducible dmeRF system from Rhizobium leguminosarum bv. viciae.* Appl Environ Microbiol, 2013. **79**(20): p. 6414-22.

461 18. Dokpikul, T., et al., *Regulation of the Cobalt/Nickel Efflux Operon dmeRF in*
462 *Agrobacterium tumefaciens and a Link between the Iron-Sensing Regulator RirA and*
463 *Cobalt/Nickel Resistance.* Appl Environ Microbiol, 2016. **82**(15): p. 4732-4742.
464 19. Li, Z., et al., *Nickel and cobalt resistance properties of Sinorhizobium meliloti isolated*
465 *from Medicago lupulina growing in gold mine tailing.* PeerJ, 2018. **6**: p. e5202.
466 20. Ranquet, C., et al., *Cobalt stress in Escherichia coli. The effect on the iron-sulfur*
467 *proteins.* J Biol Chem, 2007. **282**(42): p. 30442-51.
468 21. Thorgersen, M.P. and D.M. Downs, *Cobalt targets multiple metabolic processes in*
469 *Salmonella enterica.* J Bacteriol, 2007. **189**(21): p. 7774-81.
470 22. Macomber, L. and J.A. Imlay, *The iron-sulfur clusters of dehydratases are primary*
471 *intracellular targets of copper toxicity.* Proc Natl Acad Sci U S A, 2009. **106**(20): p. 8344-
472 9.
473 23. Fantino, J.R., et al., *A genetic analysis of the response of Escherichia coli to cobalt*
474 *stress.* Environ Microbiol, 2010. **12**(10): p. 2846-57.
475 24. Chillappagari, S., et al., *Copper stress affects iron homeostasis by destabilizing iron-*
476 *sulfur cluster formation in Bacillus subtilis.* J Bacteriol, 2010. **192**(10): p. 2512-24.
477 25. Pellicer Martinez, M.T., et al., *Sensing iron availability via the fragile [4Fe-4S] cluster of*
478 *the bacterial transcriptional repressor RirA.* Chem Sci, 2017. **8**(12): p. 8451-8463.
479 26. Martinez, M.T.P., et al., *Mechanisms of iron-and O2-sensing by the [4Fe-4S] cluster of*
480 *the global iron regulator RirA.* Elife, 2019. **8**: p. e47804.
481 27. Imlay, J.A., *Pathways of oxidative damage.* Annu Rev Microbiol, 2003. **57**: p. 395-418.
482 28. Latifi, A., M. Ruiz, and C.C. Zhang, *Oxidative stress in cyanobacteria.* FEMS Microbiol
483 Rev, 2009. **33**(2): p. 258-78.
484 29. Gao, F., *Iron-Sulfur Cluster Biogenesis and Iron Homeostasis in Cyanobacteria.* Front
485 Microbiol, 2020. **11**: p. 165.
486 30. Patel, S.J., et al., *Fine-tuning of Substrate Affinity Leads to Alternative Roles of*
487 *Mycobacterium tuberculosis Fe2+-ATPases.* J Biol Chem, 2016. **291**(22): p. 11529-39.
488 31. Brown, J.B., M.A. Lee, and A.T. Smith, *Ins and Outs: Recent Advancements in*
489 *Membrane Protein-Mediated Prokaryotic Ferrous Iron Transport.* Biochemistry, 2021.
490 **60**(44): p. 3277-3291.
491 32. Grass, G., et al., *FieF (YiiP) from Escherichia coli mediates decreased cellular*
492 *accumulation of iron and relieves iron stress.* Arch Microbiol, 2005. **183**(1): p. 9-18.
493 33. Costa, D., et al., *The Irr and RirA Proteins Participate in a Complex Regulatory Circuit*
494 *and Act in Concert To Modulate Bacterioferritin Expression in Ensifer meliloti 1021.*
495 Appl Environ Microbiol, 2017. **83**(16).
496 34. Amarelle, V., M.R. O'Brian, and E. Fabiano, *ShmR is essential for utilization of heme as*
497 *a nutritional iron source in Sinorhizobium meliloti.* Appl Environ Microbiol, 2008.
498 **74**(20): p. 6473-5.
499 35. Chao, T.C., et al., *Role of the regulatory gene rirA in the transcriptional response of*
500 *Sinorhizobium meliloti to iron limitation.* Appl Environ Microbiol, 2005. **71**(10): p. 5969-
501 82.
502 36. Cuiv, P.O., et al., *The hmuUV genes of Sinorhizobium meliloti 2011 encode the*
503 *permease and ATPase components of an ABC transport system for the utilization of*
504 *both haem and the hydroxamate siderophores, ferrichrome and ferrioxamine B.* Mol
505 Microbiol, 2008. **70**(5): p. 1261-73.
506 37. Amarelle, V., et al., *A new small regulatory protein, HmuP, modulates haemin*
507 *acquisition in Sinorhizobium meliloti.* Microbiology (Reading), 2010. **156**(Pt 6): p. 1873-
508 1882.
509 38. Amarelle, V., U. Koziol, and E. Fabiano, *Highly conserved nucleotide motifs present in*
510 *the 5'UTR of the heme-receptor gene shmR are required for HmuP-dependent*
511 *expression of shmR in Ensifer meliloti.* Biometals, 2019. **32**(2): p. 273-291.

512 39. Sato, T., et al., *The Small Protein HemP Is a Transcriptional Activator for the Hemin*
513 *Uptake Operon in Burkholderia multivorans ATCC 17616.* Appl Environ Microbiol, 2017.
514 **83**(16).
515 40. Medema, M.H., E. Takano, and R. Breitling, *Detecting sequence homology at the gene*
516 *cluster level with MultiGeneBlast.* Mol Biol Evol, 2013. **30**(5): p. 1218-23.
517 41. Simon, R., U. Priefer, and A. Puhler, *A Broad Host Range Mobilization System for In*
518 *Vivo Genetic Engineering: Transposon Mutagenesis in Gram Negative Bacteria.* Nat.
519 Biotech., 1983. **1**(9): p. 784-791.
520 42. Luo, L., et al., *Two new Sinorhizobium meliloti LysR-type transcriptional regulators*
521 *required for nodulation.* J Bacteriol, 2005. **187**(13): p. 4562-72.
522 43. Datsenko, K.A. and B.L. Wanner, *One-step inactivation of chromosomal genes in*
523 *Escherichia coli K-12 using PCR products.* Proc Natl Acad Sci U S A, 2000. **97**(12): p.
524 6640-5.
525 44. Genco, C.A., B.M. Odusanya, and G. Brown, *Binding and accumulation of hemin in*
526 *Porphyromonas gingivalis are induced by hemin.* Infect Immun, 1994. **62**(7): p. 2885-
527 92.
528 45. Martin, J.E., et al., *The Escherichia coli small protein MntS and exporter MntP optimize*
529 *the intracellular concentration of manganese.* PLoS Genet, 2015. **11**(3): p. e1004977.
530 46. Simon, R., U. Priefer, and A. Pühler, *A broad host range mobilization system for in vivo*
531 *genetic engineering: transposon mutagenesis in gram negative bacteria.*
532 Bio/technology, 1983. **1**(9): p. 784-791.
533 47. Blatny, J.M., et al., *Construction and use of a versatile set of broad-host-range cloning*
534 *and expression vectors based on the RK2 replicon.* Appl Environ Microbiol, 1997. **63**(2):
535 p. 370-9.

Table/s

Table 1. List of strains, plasmids and primers used in this study.

Strain/plasmid/primer

Strains	Relevant characteristics	Reference
Sinorhizobium meliloti		
Rm1021	Wild-type (Str^R)	[42]
Δ*aitP*	Rm1021 SMc04167::pK19mob2ΩHMB- *aitP* (Str^R) (Kan^R)	This work
Δ*mbfA*	Rm 1021 SMc00359::pJQ200SK- *mbfA* (Str^R) (Gm^R)	This work
Δ*aitP* - Δ*mbfA*	Rm 1021 SMc04167::pK19mob2ΩHMB- *aitP*; SMc00359::pJQ200SK- *mbfA*(Str^R) (Kan^R)(Gm^R)	This work
Δ*aitP*-C	Rm 1021 SMc04167::pK19mob2ΩHMB- *aitP* / pJB3Tc20-P_{770}-*aitP* (Str^R) (Kan^R) (Tc^R)	This work
Escherichia coli		
S17-1	*E. coli 294, thi RP4-2 - Tc: :Mu-Km: :Tn7* chromosomally integrated	[46]
DH5α	F- *Φ80lacZΔM15 Δ(lacZYA-argF) U169 recA1 endA1 hsdR17 (rK–, mK+) phoA supE44 λ– thi-1 gyrA96 relA1*	Invitrogen, Carlsbad, CA, USA
BL21(DE3)pLysS	F- *ompT hsdS*B (rB-mB-) *gal dcm* (DE3) *pLysS* (Cam^R)	Invitrogen, Carlsbad, CA, USA
BL21(DE3)pKD46	F- *ompT hsdS*B (rB-mB-) *gal dcm* (DE3) *pKD46* (Amp^R)	[43]
Δ*fieF*	BL21(DE3) *fieF::Km* (Kan^R)	This work
Plasmids		
pK19mob2ΩHMB	RP4 mobilizable plasmid, Kan^R	[42]
pK19mob2ΩHMB-*aitP*	SMc04167 insertion plasmid containing a 334 bp *aitP* fragment (AL591688.1:2155814-2156147)	www.rhizogate.de
pJQ200SK- *mbfA*	SMc00359 insertion plasmid containing a 568 bp *mbfA* fragment (AL591688.1:314759-315326)	This work
pJB3Tc20	Broad host-range RK2 cloning vector, Tc^R	[47]
pJB3Tc20-P_{770}-*aitP*	SMc04167 (*aitP*) containing a 770 bp promoter fragment cloned in pJB3Tc20	This work

Primers	Sequence (5'->3')	Use
qSMc02726-ShmR-F	AGCCCAACCCTACCGATTTC	qRT-PCR
qSMc02726-ShmR-R	CCTGTTCCGCTCTGAGATCA	
qSMc01512-hmuT-F	GTCTTCGGCGTTGGGAAATG	
qSMc01512-hmuT-R	GGTAAATGCTGGTGGAATCGCG	
qSMc1021-16S-F	GATAAGCCGAGAGGAAGGTG	
qSMc1021-16S-R	GTGTAGCCCAGCCCGTAAG	
qSMc04167-aitP-F	CGCGCTTTACCTTCGGTACG	
qSMc04167-aitP-R	AATGGCCTGCGGAAAACTGA	
qSMc04168-dmeR-F	GAAAAGTTGCTCGCCCGTGT	
qSMc04168-dmeR-R	GGAGGCGACGAGGTTGAGAA	
qSMc03787-bfd-F	GGACGCCGATATATTTGATTTC	
qSMc03787-bfd-R	CGTCGCCTTTCAAGATCC	
qSMc03788-bfr-F	CGATTACGTCTCGATGAAGC	
qSMc03788-bfr-R	CTGGCCGTATTTTTCCTCAC	

qSMc00359-mbfA-F	CCTCGGAAGAGGACGATGGA	
qSMc00359-mbfA-R	GCTCTCCTCCTCCGCCATTT	
qSMc00784-fbpA-F	AACTGGTTCGGTCTGACGAC	
qSMc00784-fbpA-R	AGGCCGACATTGTAGGAGTG	
qSMc00301-sufA-F	AATATGCCGTCGATCTCGTG	
qSMc00301-sufA-R	GTCTCGAAATCCATCTGCGT	
DM-F-Sma1163-BamHI	ACTGGGATCCGACAGCACCTATGCGGCA	Cloning of 600 bp and yield of double and single mutants in *S. meliloti*
DM-R-Sma1163-XhoI	CAGTCTCGAGGTCCGTATGTCTCGCGAG	
DM-F-Smc00359-BamHI	ACTGGGATCCCTGCATGTCGCCCGTTTCG	
DM-R-Smc00359-XhoI	CAGTCTCGAGCGAGTGCCGTCATGATGC	
BamHI_AitP_-770_FW	GGGGATCCCCTCCCAGGCTAAAGCACGT	Complementation in *trans*
PstI_aitP_Stop_RV	GGCTGCAGCTCAGGCCGCCAGCGGCTCG	
Delta-fieF-F	ATGAATCAATCTTATGGACGGCTGGTCAGTCGGGCGGCGATTGCTGCGACGTGTAGGCTGGAGCTGCTTC	Generating *E. coli* Δ*fieF*
Delta-fieF-R	TTATGAAAGCATAGACCGTTTACCCTCCCTGGGTACGACGGAACAGGGGTCATATGAATATCCTCCTTAG	

537

Figure legends

Figure 1. AitP is involved in Co^{2+} homeostasis and genetic context of bacterial AitP-like transporters point to a broader transport specificity and regulation. A) Operon architecture analysis of AitP-like transporters in bacterial sequenced organisms indicates the existence of a subgroup with different transcriptional regulation. B) Metal toxicity was evaluated by inhibition halo assay using *S. meliloti* Rm1021 and Δ*aitP*. 7-mm filter paper discs containing 10 (up-left), 5 (up-right), 2 (down-left) or 1 (down-right) mmole of the indicated metal (as Cl^- except for $FeSO_4$), were dried and then laid on top of a soft-agar inoculated with each strain (OD_{600nm}=0.05). Plates were incubated 48 h at 30°C and inhibition halo diameters were compared between strains. Broken circle with same diameter was lay on top of the image for comparison. Notice the Co^{2+} sensitivity in Δ*aitP*. C) Serial dilutions (10 µl) of cells initially at OD_{600nm}=0.4 were spotted on TY-agar supplemented with the indicated Co^{2+} (as Cl^-) concentration for 48 h at 30°C.Complementation was achieved by transformation of Δ*aitP* with pJB3Tc20-P_{770}-*aitP*. Notice that Co^{2+} sensitivity was restored to WT levels in Δ*aitP*-C strain. D) Cobalt content in cells after incubation with 0.2 mM CoCl2 for 1 hour at 30°C in TY medium during early exponential phase growth. E) Fold change expression levels ($2^{-\Delta\Delta Ct}$ with 16S as reference gene), of *dmeR*, *aitP* and *mbfA* with Co^{2+} or F) Fe^{2+} treatment. Cells were grown till mid-log phase at 30°C in TY. At this point media were supplemented accordingly and incubated for 45 min at 30°C before RNA extraction. Data are the mean ± SE of three independent experiments. * = $p < 0.05$ and # = $p<0.01$ from a two tail Student's t-test of averaged ΔC_t (treated *vs.* non-treated/Bpy).

Figure 2. AitP transports Fe with low affinity and high specificity. Fe^{2+} uptake was measured in energized everted membrane vesicles obtained from *E. coli* Δ*yiiP* expressing AitP. Previous to transport measurements vesicles were energized by 2-minute pre-incubation with 2.5 mM NADH at 37°C and the uptake was initiated by addition of a 10-fold concentrated $^{59}Fe^{2+}$ solution and mixing. Reaction was stopped after 5-minute incubation at the same temperature by filtering through 0.22 µm nitrocellulose.

Filters were immediately washed with a standard solution containing 2 mM EDTA and dissolved in scintillation cocktail for counting (see materials and methods). A) Fe^{2+} transport kinetics. Data were fitted to $v = V_{max}\,[Fe^{2+}]/\,K_{1/2} + [Fe^{2+}]$ equation by using $K_{1/2}$ = 1.35±0.21 mM and V_{max} = 16.4±1.0 nmol.mg^{-1}.min^{-1}. B) Apparent effects on Fe^{2+} transport rate by AitP of unlabeled divalent transition metals (TM^{2+}) as real substrates or competitive inhibitors. Dashed line depicts the expected transport rate value obtained using $v = V_{max}\,[Fe^{2+}]/\,(K_{1/2}\,(1+([TM^{2+}]/K_i))+[Fe^{2+}])$, with $[Fe^{2+}]=[TM^{2+}]=$ 2 mM and K_i assumed to be equal to $K_{1/2}$. Note that only Co^{2+} affects negatively the Fe^{2+} transport rate probably as real substrate. In all cases, Fe^{2+} uptake by vesicles from empty vector transformed strain *E. coli* Δ*fieF* was subtracted prior to data analysis. In all cases data are the mean ± SE of three independent experiments.

Figure 3. AitP is involved in Fe^{2+} homeostasis. A) Serial dilutions (10 µl) of *S. meliloti* Rm1021, Δ*aitP,* Δ*nia,* Δ*mbfA*, Δ*aitP* - Δ*nia* and Δ*aitP*-Δ*mbfA* cells initially at OD_{600nm}=0.4 were spotted on TY-agar supplemented with the indicated Co^{2+} (as Cl^-) concentration for 48 h at 30°C. B) Cobalt content in Rm1021, Δ*aitP,* Δ*aitP* - Δ*nia* and Δ*aitP*-Δ*mbfA* after incubation with 0.2 or 0.5 mM Co^{2+} for 1 hour at at 30°C in TY medium during early exponential phase growth. C) Serial dilutions (10 µl) of *S. meliloti* Rm1021, Δ*aitP,* and Δ*aitP* with pJB3Tc20-P_{770}-*aitP,* cells initially at OD_{600nm}=0.4 were spotted on TY-agar supplemented with the indicated Co^{2+} (as Cl^-) and Fe^{2+} (as SO_4^{2-}) concentration for 48 h at 30°C. D) Fold change expression levels ($2^{-\Delta\Delta Ct}$ with 16S as reference gene) of *fbpA*. Cells were grown till mid-log phase at 30°C in TY. At this point media were supplemented with 200 µM $CoCl_2$ and incubated for 45 min at 30°C before RNA extraction E) Total heme was estimated after cell incubation with 0.2 mM $CoCl_2$ for 2 hours at 30°C during exponential growth phase. Data points and the mean of three independent experiments are shown. * = $p < 0.05$. F) Fold change expression levels ($2^{-\Delta\Delta Ct}$ with 16S as reference gene) of *sufA*. Cells were grown till mid-log phase at 30°C in TY. At this point media were supplemented accordingly and incubated for 45 min at 30°C before RNA extraction. For

D) and F) Data are the mean ± SE of three independent experiments. * = $p < 0.05$ and # = $p<0.01$ from a two tail Student's t-test of averaged ΔC_t (treated *vs.* non-treated).

Figure 4. AitP activity induces heme uptake transport. A) Fold change expression levels ($2^{-\Delta\Delta Ct}$) of heme uptake components in WT (light gray) and Δ*aitP* (dark gray) *in vitro vs.* 16S reference gene. Cells were grown till mid-log phase at 30°C in TY. After this a half of the culture volume was supplemented with $CoCl_2$ or nothing, and incubated for 2 hours at 30°C before RNA extraction. Data are the mean ± SE of four independent experiments. * = $p < 0.05$ and # = $p<0.01$ from a two tail Student's t-test of averaged ΔC_t (treated *vs.* non-treated).B) Serial dilution spots (10 µl) of *S. meliloti* Rm1021, Δ*aitP,* and Δ*aitP* with pJB3Tc20-P_{770}-*aitP,* cells initially at OD_{600nm}=0.4 were spotted on TY-agar supplemented with the indicated Co^{2+} (as Cl^-) and hemin concentration for 48 h at 30°C. C) Serial dilutions (10 µl) of *S. meliloti* Rm1021, Δ*aitP,* and Δ*aitP* with pJB3Tc20-P_{770}-*aitP,* cells initially at OD_{600nm}=0.4 were spotted on TY-agar supplemented with the indicated Co^{2+} (as Cl^-) and 200 µM PPIX or 200 µM hemin concentration for 48 h at 30°C. D) Hemin uptake assay of WT (light gray) and Δ*aitP* (dark gray) cells. Different letters designate significantly different means as informed by a Bonferroni post hoc ($p < 0.05$) test of an ANOVA. E) Cells were grown in TY at 30°C till mid-exponential phase and then incubated with Co^{2+} and hemin concentrations as indicated for 2 hours (n=2). After several washes pellets were imaged. Notice the green darker color of Rm1021 cells (down-left) after the Co^{2+}+hemin incubation *vs.* Δ*aitP,* indicating increased hemin accumulation. Pictures show representative results of at least three independent experiments.

Figure 1

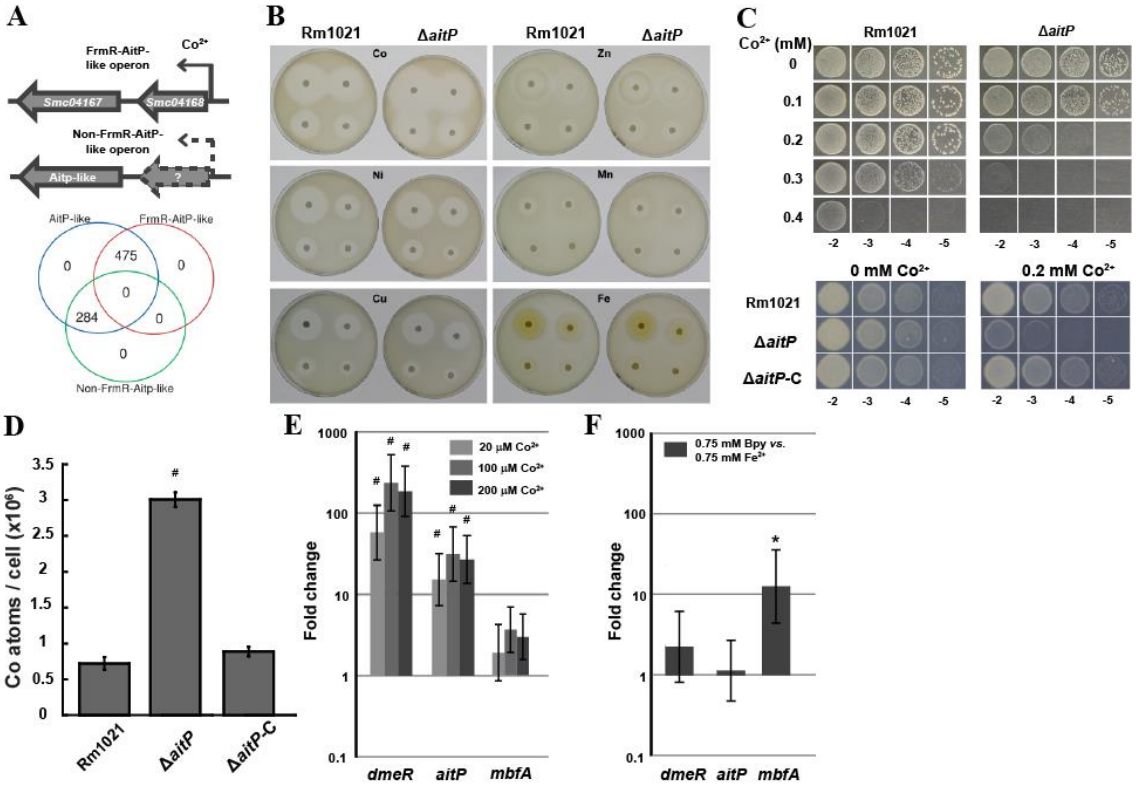
A
FrmR-AitP-like operon
Co2+
Smc04167
Smc04168
Non-FrmR-AitP-like operon
Aitp-like
?
AitP-like
FrmR-AitP-like
Non-FrmR-Aitp-like
475
284
0
B
Rm1021
ΔaitP
Co
Zn
Ni
Mn
Cu
Fe
C
Co2+ (mM)
0
0.1
0.2
0.3
0.4
-2
-3
-4
-5
0 mM Co2+
0.2 mM Co2+
Rm1021
ΔaitP
ΔaitP-C
D
Co atoms / cell (x10⁶)
Rm1021
ΔaitP
ΔaitP-C
E
Fold change
20 µM Co2+
100 µM Co2+
200 µM Co2+
dmeR
aitP
mbfA
F
0.75 mM Bpy vs. 0.75 mM Fe2+
Fold change
dmeR
aitP
mbfA

Figure 2

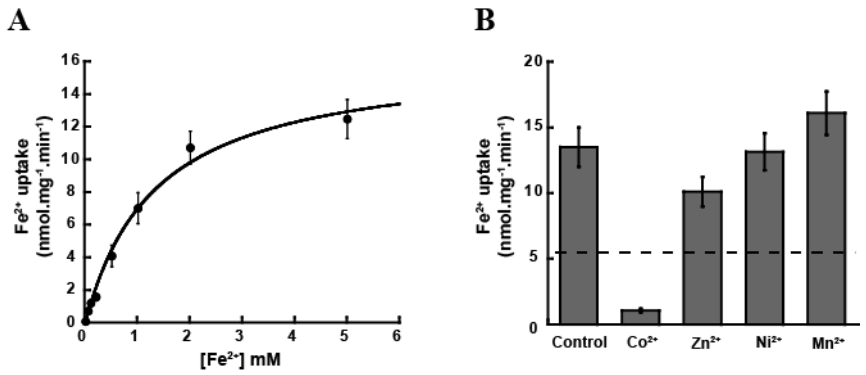

Figure 3

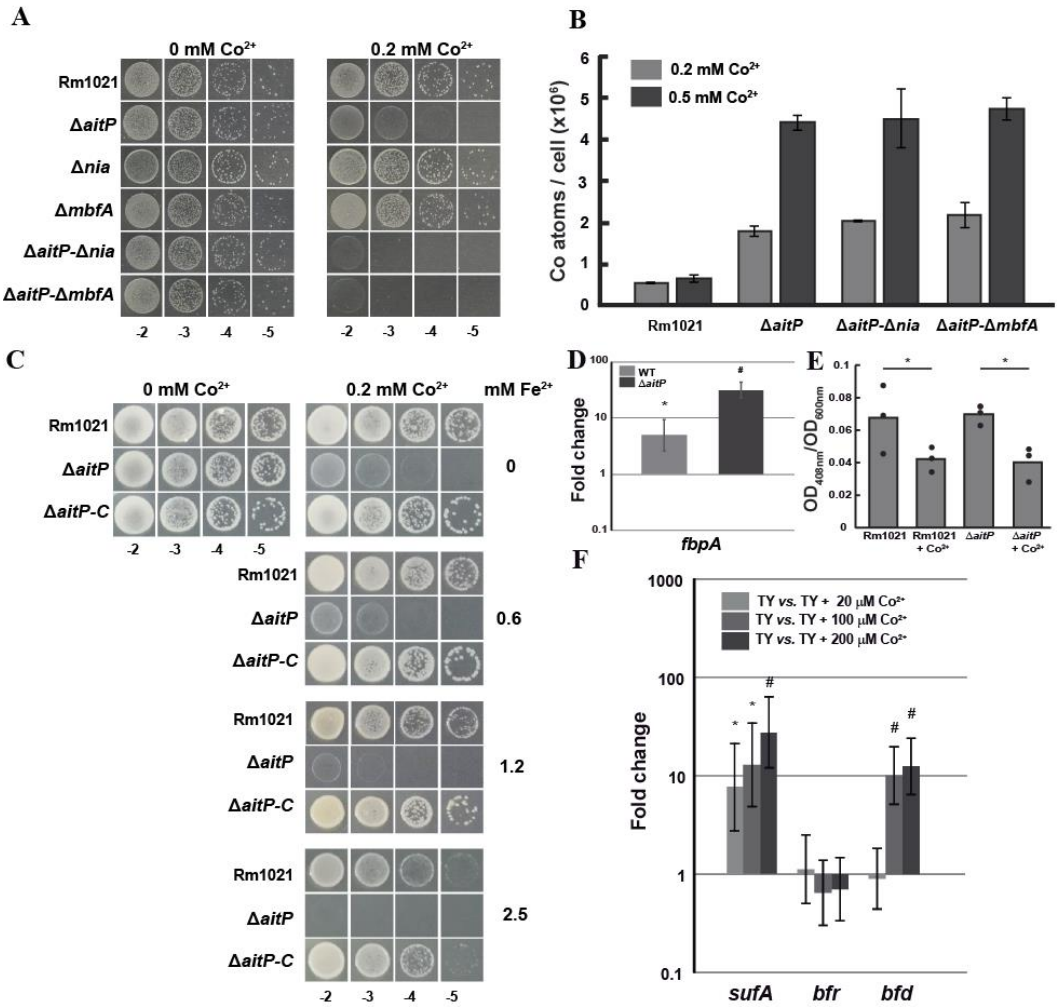
A
0 mM Co2+
0.2 mM Co2+
Rm1021
ΔaitP
Δnia
ΔmbfA
ΔaitP-Δnia
ΔaitP-ΔmbfA
-2 -3 -4 -5
B
0.2 mM Co2+
0.5 mM Co2+
Co atoms / cell (x10^6)
Rm1021
ΔaitP
ΔaitP-Δnia
ΔaitP-ΔmbfA
C
0 mM Co2+
0.2 mM Co2+
mM Fe2+
ΔaitP-C
0
0.6
1.2
2.5
D
WT
ΔaitP
Fold change
fbpA
E
OD408nm/OD600nm
Rm1021
Rm1021 + Co2+
ΔaitP
ΔaitP + Co2+
F
TY vs. TY + 20 μM Co2+
TY vs. TY + 100 μM Co2+
TY vs. TY + 200 μM Co2+
Fold change
sufA
bfr
bfd

Figure 4

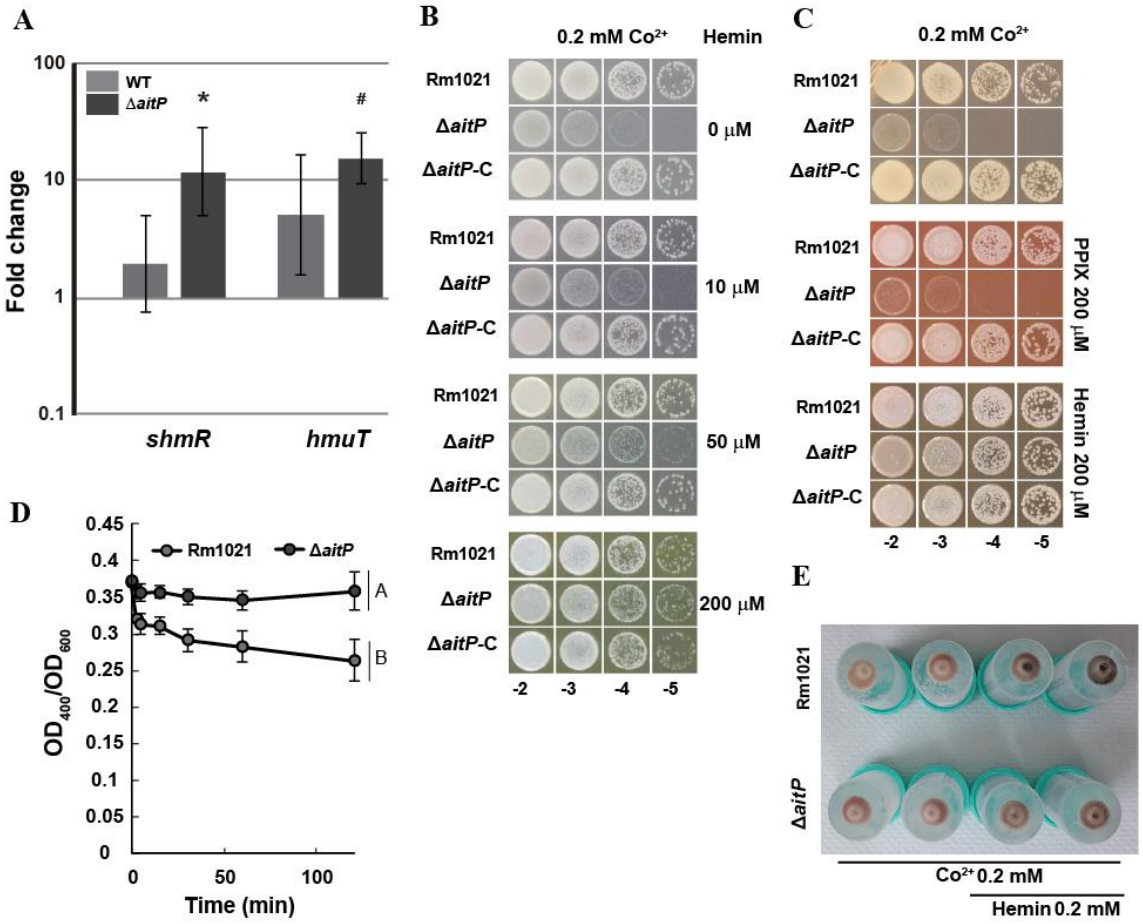
A
WT
ΔaitP
Fold change
100
10
1
0.1
*
#
shmR
hmuT
B
0.2 mM Co2+
Hemin
Rm1021
ΔaitP
ΔaitP-C
0 μM
10 μM
50 μM
200 μM
-2
-3
-4
-5
C
0.2 mM Co2+
PPIX 200 μM
Hemin 200 μM
D
Rm1021
ΔaitP
OD400/OD600
Time (min)
A
B
E
Rm1021
ΔaitP
Co2+ 0.2 mM
Hemin 0.2 mM